International Journal of Solids and Structures 50 (2013) 2659–2666

Contents lists available at SciVerse ScienceDirect

International Journal of Solids and Structures

journal homepage: www.elsevier.com/locate/ijsolstr

Adhesion model of side contact for an extensible elastic fiber

L.W. He [a], S.P. Yan [b], B.Q. Li [a], G. Zhao [a], J.R. Chu [a,*]

[a] Department of Precision Machinery and Precision Instrumentation, School of Engineering Science, University of Science and Technology of China, Hefei, Anhui, PR China
[b] CAS Key Laboratory of Mechanical Behavior and Design of Materials, University of Science and Technology of China, Hefei, Anhui, PR China

ARTICLE INFO

Article history:
Received 10 August 2012
Received in revised form 30 March 2013
Available online 30 April 2013

Keywords:
Directional adhesion
Extensible Euler Bernoulli beam
Normal pull-off force
Pre-tension
Adhesion stability

ABSTRACT

For accurately predicted adhesion laws of fibrillar structures contribute to the rational design of high-performance biomimetic adhesives, an adhesion model is proposed to study the directional adhesion behavior of an extensible elastic fiber that contacts a rigid smooth surface with its side surface under the coupling effect of normal and shear forces, based on the extensible Euler Bernoulli beam theory and the surface energy concept. The deformed configuration of the fiber is obtained analytically, and on the basis of this result, the detachment mode and the normal pull-off force of the fiber for a given shear force are predicted directly. It is also found that, due to the extensibility of the fiber, there exists a maximum normal pull-off force (MNPF) when an optimal shear force is applied. The MNPF will be enhanced by increasing the axial stiffness, and reduced by increasing the bending stiffness. In addition, generating an optimal pre-tension in the adhered part of the fiber will maximize the MNPF. The derived adhesion law is expected to contribute to the optimal design and applications of single-level fibrillar adhesives.

1. Introduction

Many animals, particularly geckos, have excellent climbing capabilities on almost any rough surfaces. This phenomenon has attracted lots of research interests in recent decades (Autumn et al., 2002; Federle et al., 2002). It is revealed that some of these animals evolve microfiber or hierarchical fiber arrays (Arzt et al., 2003; Jagota and Bennison, 2002; Varenberg et al., 2010) on their feet for strong attachment and easy detachment functions. These facts stimulate a big demand of biomimetic and bio-inspired innovations in developing high-performance synthetic adhesives (del Campo et al., 2007; Jeong et al., 2009; Kim et al., 2009; Murphy et al., 2009; Yoon et al., 2009), which in turn leads to particular research enthusiasms in the adhesion behavior of micro/nano fibers on solid surfaces, such as the adhesion of a vertical/slanted fiber with a flat surface using its top-tip (Carbone et al., 2011; del Campo et al., 2007; Gao and Yao, 2004; Hui et al., 2004), or through its side surface (He et al., 2012; Jeong et al., 2010; Lee et al., 2008; Majidi et al., 2005; Majidi, 2009; Qu et al., 2008). Geckos' adhesion behavior also arouses extensive body of work on peeling problems related to the adhesion of fibrillar adhesives (Chen et al., 2009; Cheng et al., 2012; Peng et al., 2010; Pesika et al., 2007; Tian et al., 2006).

The adhesion of a fiber with a flat surface utilizing its top-tip has been intensively studied. Contact splitting principle for such a type of adhesion is first discovered (Arzt et al., 2003), and then size effect (Gao and Yao, 2004; Hui et al., 2004) and shape effect (Carbone et al., 2011; del Campo et al., 2007) of the tip on the adhesion behavior are clarified. Though these findings help design fibrillar adhesives with strong normal adhesion strength, this type of adhesion usually does not provide the directional adhesion property found in the geckos' adhesion test (Autumn et al., 2006) and many synthetic adhesives (Jeong et al., 2010; Lee et al., 2008; Qu et al., 2008). To solve that problem, side-contact adhesion models (with a fiber's side surface contacting a surface) are proposed to explain the mechanism for the directional adhesion property (He et al., 2012; Majidi, 2009), which allows for strong attachment and easy detachment by solely applying sufficient shear forces along two opposite directions. In fact, it is by utilizing the side-contact adhesion that lots of researches and developments have been carried out to achieve the property (Jeong et al., 2010; Lee et al., 2008; Soto et al., 2010). Although another kind of models, film peeling models, explains the directional adhesion behavior of a thin film (Chen et al., 2009; Cheng et al., 2012; Kendall, 1975; Peng et al., 2010; Pesika et al., 2007; Tian et al., 2006), the prediction of these natural and synthetic adhesives with relatively complex structures requires more practical models. In accordance with the above analyses, our research is focused on developing

Abbreviations: AR, aspect ratio; CLJSC, critical line of jumping-off side contact; CLSC, critical line of side contact; CLSCWJ, critical line of side contact without jumping; ESCM, extensible side contact model; ISCM, inextensible side contact model; MNPF, maximum normal pull-off force.

* Corresponding author. Tel.: +86 551 3602544; fax: +86 551 3607504.
E-mail address: jrchu@ustc.edu.cn (J.R. Chu).

0020-7683/$ - see front matter © 2013 Published by Elsevier Ltd.
http://dx.doi.org/10.1016/j.ijsolstr.2013.04.018

side-contact model for adhesives, such as those with single-level fibrillar structures.

In terms of side contact problems, Majidi et al. (2005) and Majidi (2009) studied the side contact mechanism of a fiber on a flat surface under the effect of a normal or shear force. They found that the slanted angle of the fiber increases the contact length and that the adhesion is aided by the application of a shear load to the base of the fiber. These theoretical results are supported by recent experimental findings (Jeong et al., 2010; Lee et al., 2008; Soto et al., 2010). However, their experiments also found that the normal pull-off force increases with the applied shear force, for theoretical examinations of this behavior must address the coupling between the shear and normal loadings. According to the study on the coupling effect of the adhesion in our previous paper (He et al., 2012), the law of directional adhesion is obtained analytically and eligible of direct comparison with their experimental outcomes. It should be noted that all the work assumes that the fiber is inextensible, when large error in predicting the adhesion behavior for soft fibers might be produced. The prediction error brought by neglecting the axial deformation is similar to that of the Rivlin model (1944) relative to the Kendall model (1975). According to the studies of Chen et al. (2009) and Cheng et al. (2012), the generation of a constant or non-uniform pre-tension in the adhered film will significantly increase the angle dependence of the peel-off force, and thus the directional adhesion property. Since bending deformation is inevitable, the effect of pre-tension should be revisited when both the axial stiffness and bending stiffness are considered.

In this paper, we aim to disclose the directional adhesion law of the fiber from an extensible side contact model (ESCM), in which both the axial and bending deformation of the fiber are simultaneously taken into account. Firstly the governing equation and the adhesion boundary condition are derived via a variational method; then an analytical formula for the deformed configuration of the fiber is obtained. Based on that formula, the directional adhesion law is further predicted. By comparing the ESCM with the available Rivlin model (1944), Kendall model (1975) and the inextensible side contact model (He et al., 2012), the applicable conditions of these models are determined. The effects of the axial and bending stiffness on the adhesion behavior, together with the influence of the pre-tension generated in the adhered part of the fiber, are discussed in detail.

2. Modeling

As shown in Fig. 1, we study a single extensible straight fiber in side contact with a rigid smooth surface. A large enough preload in the normal direction can ensure that side contact exists (Majidi et al., 2005). The fiber's length is l, slanted angle α, bending stiffness EI with Yong's modulus E and inertia moment I, and axial stiffness EA with cross-sectional area A. Due to the axial strain caused by the applied normal force F_n and shear force F_t, the length of the non-contact part of the fiber a' could be different from that in the original configuration, which is termed as "non-contact length" and denoted by $a(a < l)$. The equivalent energy of adhesion per unit length on the contact interface is denoted by ω (Majidi et al., 2005). We are mainly interested in the process of losing contact, i.e. increasing a. The pre-tension that may be generated during the attachment/healing process in the adhered part of the fiber is not considered in the derivation in Section 2.1, but will be taken into account in Section 2.4.

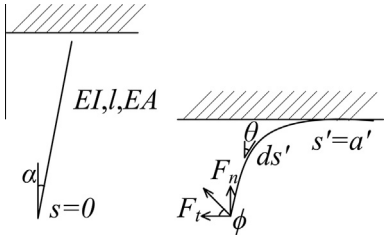

Fig. 1. A straight extensible fiber contacts with a rigid smooth surface.

2.1. Model derivation

The total free energy of the system U contains four parts, which are the bending energy of the fiber U_B, the axial deformation energy of the fiber U_A, the surface energy U_S and the potential of the external force U_P respectively. By using an coordinate (s', θ) established along the arc length of the deformed fiber as sketched in Fig. 1, the expressions of these energies are as follows (Johnson, 1985; Timoshenko and Gere, 1962):

$$\begin{aligned} U_B &= \int_0^{a'} \frac{1}{2} EI \left(\frac{\partial \theta}{\partial s'}\right)^2 ds', \\ U_A &= \int_0^{a'} \frac{1}{2} EA \left(\frac{F_{ten}}{EA}\right)^2 ds', \\ U_S &= -(l-a)\omega, \\ U_P &= -F_t \left[(l-a) + \int_0^{a'} \sin\theta ds'\right] + F_n \int_0^{a'} \cos\theta ds', \end{aligned} \tag{1}$$

where

$$F_{ten} = F_t \sin\theta - F_n \cos\theta. \tag{2}$$

Formulating the problem in the convected coordinate (s, θ) initially established along the arc length of the undeformed configuration, and using a relation between the microelements in the two coordinates (s', θ) and (s, θ),

$$ds' = \left(1 + \frac{F_{ten}}{EA}\right) ds, \tag{3}$$

under the assumption of small axial strain ($\varepsilon_{axial} \ll 1$), we can approximately derive the total energy of the system as:

$$\begin{aligned} U_T = &\int_0^a \frac{1}{2} EI \left(\frac{\partial \theta}{\partial s}\right)^2 ds - \int_0^a \frac{1}{2} EA \left(\frac{F_{ten}}{EA}\right)^2 ds \\ &- F_t \left[(l-a) + \int_0^a \sin\theta ds\right] + F_n \int_0^a \cos\theta ds - (l-a)\omega. \end{aligned} \tag{4}$$

Comparison of the above equation with that of the inextensible case (He et al., 2012) shows that the axial deformation results in a decrease of the total energy of the system with a quantity equal to the axial strain energy. This is because the decrease of the potential energy of the external forces caused by the axial deformation is the double of the axial strain energy, resulted from the linear elastic mechanics. Here the relative error of the energy approximation is of the order of the maximum axial strain.

At equilibrium, the total free energy of the system reaches its minimum, requiring that the variational derivatives of U_T with respect to θ and a vanish. Applying a variational method to Eq. (4), we are able to obtain the equilibrium equation and the adhesion boundary condition of the system

$$\begin{aligned} &EI \frac{\partial^2 \theta}{\partial s^2} + (F_n \sin\theta + F_t \cos\theta)\left(1 + \frac{F_t \sin\theta - F_n \cos\theta}{EA}\right) = 0, \quad 0 \leqslant s \leqslant a, \\ &\frac{1}{2} EI \left(\frac{\partial \theta}{\partial s}\right)^2 + \frac{1}{2} EA \left(\frac{F_{ten}}{EA}\right)^2 = \omega, \quad s = a, \end{aligned} \tag{5}$$

with the natural boundary conditions

$$\begin{aligned} &\theta(0) = \alpha, \\ &\theta(a) = \frac{\pi}{2}. \end{aligned} \tag{6}$$

Comparisons of these equations with that of the inextensible case (He et al., 2012) show that owing to the axial deformation, a new term comes into the governing equation and the adhesion criterion $G = \omega$ (G, the energy release rate of the fiber) at the contact boundary is also modified. The new term represents a new shear force acting on the cross-section and is actually the derivative of the axial strain energy per unit length with respect to θ. The derived governing equation is the same with that given by Liu (2009) who derived it from the force-equilibrium method. It is easy to find that Eq. (5) degenerates to the equation of the inextensible case (He et al., 2012) if EA approaches to infinity. Thus the inextensible side contact model (ISCM) is a limit of the ESCM.Using the two side contact models, we can also address the problem of peeling a fiber from a rigid substrate by changing the boundary condition from $\theta(0) = \alpha$ to $\theta'(0) = 0$. In this case, it is easy to find that if the bending stiffness approaches to zero, the ESCM and ISCM will be identical to the Kendall and Rivlin model respectively. More importantly, the two side contact models could predict the adhesion behavior of a fiber constrained on a rigid support with a fixed angle, which is our main interest. Therefore, we are able to conclude that all the other three models are degenerate versions of the newly developed model. Taken the more rigorous new model as a reference, its comparison with the other models allows for determining their respective applicable conditions.

2.2. Deformation analysis

Integrating the first expression in Eq. (5), we have:

$$\frac{1}{2}EI\theta'^2 = -F_t\sin\theta + F_n\cos\theta - \frac{(F_t\sin\theta - F_n\cos\theta)^2}{2EA} + M, \tag{7}$$

where M is an independent variable that does not depend on s and its specific value for the equilibrium state will be given below.

Introducing the following variables:

$$N = \sqrt{F_t^2 + F_n^2}, \quad \tan\phi = \frac{F_n}{F_t}, \quad c = \frac{\omega}{EA}, \tag{8}$$

we can transform Eq. (7) to the following integral form through simple calculations,

$$\bar{a} = \sqrt{\frac{EI}{\omega l^2}}\int_{\alpha}^{\pi/2}\frac{d\theta}{\sqrt{\bar{N}^2 c\sin^2(\theta-\phi) - 2\bar{N}\sin(\theta-\phi) + 2\bar{M}}}, \tag{9}$$

where $\bar{M} = M/\omega$, $\bar{N} = N/\omega = \sqrt{\bar{F}_n^2 + \bar{F}_t^2}$, $\bar{a} = a/l$, $\bar{F}_t = F_t/\omega$, $\bar{F}_n = F_n/\omega$. Within Eq. (9), $EI/\omega l^2$ means the dimensionless bending stiffness; c stands for the dimensionless axial compliance; $\bar{F}_t$ and $\bar{F}_n$ denote the dimensionless shear and normal forces respectively. Eq. (9) also shows that a is a monotonically decreasing function of M.By using the substitution of variables $t = \frac{\pi}{4} + \frac{\theta-\phi}{2}$, Eq. (9) can be rewritten as:

$$\bar{a} = \sqrt{\frac{EI}{\omega l^2}}\int_{\pi/4+\alpha/2-\phi/2}^{\pi/2-\phi/2} \times \frac{2dt}{\sqrt{2\bar{M}(1+q-p)[(1-\lambda_1\sin^2 t)(1+\lambda_2\sin^2 t)]}}, \tag{10}$$

where $q = \bar{N}/\bar{M}, p = \bar{N}^2 c/(2\bar{M})$, and

$$\lambda_1 = \frac{(q-2p) + \sqrt{q^2+4p}}{1+q-p}, \quad \lambda_2 = \frac{-(q-2p) + \sqrt{q^2+4p}}{1+q-p}. \tag{11}$$

By following the method adopted by Magnusson et al. (2001), the integral in Eq. (10) can be reduced to an elliptical integral on Legendre's normal form (also called as the elliptical integral of the first kind $F(x,m)$) through the following substitution of variables:

$$\sin^2 t = \frac{\sin^2\varphi}{(1+\lambda_2) - \lambda_2\sin^2\varphi}.$$

It is straightforward to check that this transformation is invertible.

With this substitution, Eq. (10) can be expressed as:

$$\bar{a} = \sqrt{\frac{2EI}{\omega l^2}}\frac{1}{\sqrt{\bar{M}(1+q-p)(1+\lambda_2)}}\int_{\varphi_1}^{\varphi_2}\frac{d\varphi}{\sqrt{1-m\sin^2\varphi}} = \sqrt{\frac{2EI}{\omega l^2}}\frac{1}{\sqrt{\bar{M}(1+q-p)(1+\lambda_2)}}[F(\varphi_2,m) - F(\varphi_1,m)], \tag{12}$$

where

$$m = \frac{\lambda_1+\lambda_2}{1+\lambda_2}, \quad \varphi_2 = \varphi(\pi/2), \quad \varphi_1 = \varphi(\alpha)$$

and

$$\varphi(\theta) = \begin{cases} \mathrm{Arcsin}\left[\sqrt{\frac{(1+\lambda_2)(1+\sin(\theta-\phi))}{2+\lambda_2(1+\sin(\theta-\phi))}}\right], & \theta-\phi > \frac{\pi}{2} \\ \pi - \mathrm{Arcsin}\left[\sqrt{\frac{(1+\lambda_2)(1+\sin(\theta-\phi))}{2+\lambda_2(1+\sin(\theta-\phi))}}\right], & \theta-\phi \leqslant \frac{\pi}{2} \end{cases}$$

The deformed configuration of the fiber can also be obtained as:

$$\bar{s} = \sqrt{\frac{2EI}{\omega l^2}}\frac{1}{\sqrt{\bar{M}(1+q-p)(1+\lambda_2)}}\int_{\varphi_1}^{\varphi(\theta)}\frac{d\varphi}{\sqrt{1-m\sin^2\varphi}} = \sqrt{\frac{2EI}{\omega l^2}}\frac{1}{\sqrt{\bar{M}(1+q-p)(1+\lambda_2)}}[F(\varphi(\theta),m) - F(\varphi_1,m)]. \tag{13}$$

When the system is at equilibrium, substituting Eqs. (5) and (6) into Eq. (7), we have $M = \hat{M} = Ft + \omega$; the non-contact length at equilibrium $a = \hat{a}$ can also be obtained by substituting the expression of $\hat{M}$ into Eqs. (9), (12). Thus it is easy to find that if EA approaches to infinity, the formula (Eq. (12)) for the equilibrium non-contact length degenerates to that of the inextensible case (He et al., 2012).

2.3. Directional adhesion law of the extensible fiber

Based on the formulas derived in Section 2.2, the directional adhesion law of the fiber contacting with a rigid flat surface will be predicted. By utilizing the non-negativity condition of the bending strain energy (shown in Eq. (7)) that we once used (He et al., 2012), the equations for the critical line of jumping-off side contact (CLJSC) of the fiber are obtained analytically as given below (Eqs. (14) and (15)). The critical line is also depicted in a 2D force space as shown in Fig. 2. The upper part of the CLJSC is the same with that predicted by the Kendall model (Eq. (14)) and it depends only on the axial stiffness, while the lower part relies on α besides the axial stiffness (Eq. (15)). Two horizontal critical lines are also shown in Fig. 2, which physically denote the slip failure modes dominated by the stretching and compressing deformation respectively (Eq. (16)).

$$\left(\sqrt{\bar{F}_t^2 + \bar{F}_n^2} - \bar{F}_t\right) + \frac{c}{2}\left(\bar{F}_t^2 + \bar{F}_n^2\right) - 1 = 0, \tag{14}$$

$$\left[\left(\bar{F}_t\sin\alpha - \bar{F}_n\cos\alpha\right) - \bar{F}_t\right] + \frac{c}{2}\left(\bar{F}_t\sin\alpha - \bar{F}_n\cos\alpha\right)^2 - 1 = 0, \tag{15}$$

$$\bar{F}_t = \pm\sqrt{\frac{2}{c}}. \tag{16}$$

By assuming that when $\bar{a} = 1$ the fiber loses side contact without jumping, the critical line of side contact without jumping (CLSCWJ)

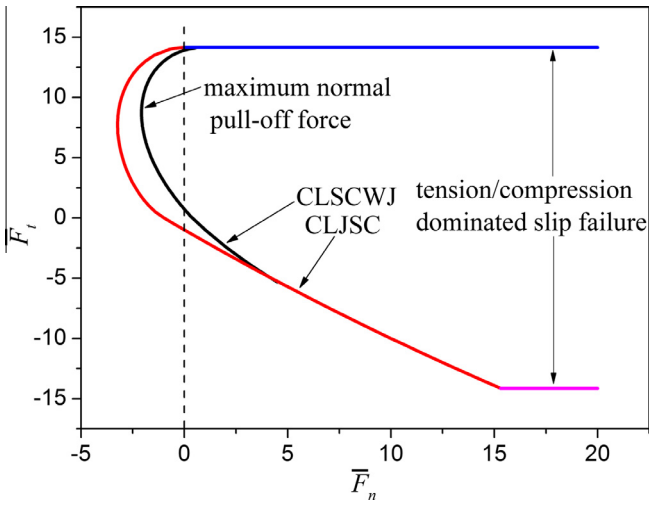

Fig. 2. The critical line of jumping off side contact (CLJSC), the critical line of side contact without jumping (CLSCWJ, contour of $\bar{a}=1$) and the critical lines of slip failure in a 2D force space are depicted in the figure where $EI/\omega l^2 = 1$, $EA/\omega = 100$ and $\alpha = 0$.

in the 2D force space can also be obtained. Moreover, if the critical normal pull-off force for a given shear force is negative, the fiber will detach from the contacting surface. Therefore as shown in Fig. 2, the actual critical line of side contact (CLSC) consisting of the CLSCWJ, part of the CLJSC and part of the critical lines of slip failure represents the boundary of possible adhesion equilibrium states in the 2D force space. It means physically that if the applied force is within the region bounded by the CLSC, detachment won't take place; but once it meets one of these lines, the fiber will detach in the corresponding manner (non-jumping detachment, jumping detachment or slip failures). Similar to the case of the ISCM, the exact position of the CLSC relies on the bending stiffness and α. However, a significant difference is that, due to the extensibility of the fiber, there exists a maximum normal pull-off force (MNPF) when an optimal shear force is applied as shown in Fig. 2.

Furthermore, the stability of available adhesion equilibrium states can be determined by using a stability criterion of energy minimization. It turns out that all the equilibrium states are stable. A provement similar to that of the inextensible case (He et al., 2012) is adopted and details of the provement are given in the appendix.

2.4. Pre-tension effect on the adhesion behavior

In this study, it is also found that the influence of pre-tension on the adhesion behavior, which may exist in the adhered part of the fiber, can be naturally incorporated into our model. Through a procedure of formulating the total energy of the system and performing a variational analysis similar to that in Section 2.1, we are able to derive that the presence of pre-tension in the adhered part of the fiber does not necessitate changing the governing equation, but only leads to modifying the adhesion boundary condition to the following form:

$$\frac{1}{2}EI\left(\frac{\partial\theta}{\partial s}\right)^2+\frac{1}{2}EA\left(\frac{F_{ten}-F_{pre}}{EA}\right)^2=\omega,\quad s=a, \tag{17}$$

From this equation we are able to conclude that in the case of $\theta(a)=\pi/2$, when the fiber is dragged in the positive direction ($F_t>0$), generating a pre-tension of a certain magnitude ($0<F_{pre}<2F_t$) in advance on the contact interface will decrease the energy release rate (the left-hand side of Eq. (17)), thus promoting the adhesion performance. The analytical formula for the non-contact length will also be obtained just by modifying the value of $\hat{M}$ from $(F_t+\omega)$ to $[F_t+\omega+(2F_t-F_{pre})F_{pre}/(2EA)]$. Hence the directional adhesion law in this case can also be formulated by following the method given in Section 2.3. Equations for the corresponding CLJSC and critical lines of slip failure in this case are given below:

$$\left(\sqrt{\overline{F}_t^2+\overline{F}_n^2}-\overline{F}_t\right)+\frac{c}{2}\overline{F}_n^2+\frac{c}{2}\left(\overline{F}_t-\overline{F}pre\right)^2-1=0, \tag{18}$$

$$\left[\left(\overline{F}_t\sin\alpha-\overline{F}_n\cos\alpha\right)-\overline{F}_t\right]+\frac{c}{2}\left[\left(\overline{F}_t\sin\alpha-\overline{F}_n\cos\alpha\right)^2-\overline{F}_t^2\right]+\frac{c}{2}\left(\overline{F}_t-\overline{F}_{pre}\right)^2-1=0, \tag{19}$$

$$\overline{F}_t=\overline{F}_{pre}\pm\sqrt{\frac{2}{c}}. \tag{20}$$

When $\overline{F}_n\ll\overline{F}_t$, Eq. (18) predicts the same result of the generalized Kendall model that describes the effect of pre-tension on the peeling behavior of an extensible film (Chen et al., 2009). To accurately predict the critical line of adhesion for a comparatively stiff fiber, the implicit equation $\bar{a}=1$ has to be solved, which is similar to the pre-tension free case. Thus different from the generalized Kendall model (Chen et al., 2009), our model includes the influence of the bending stiffness and is applicable to fibers/films constrained on a rigid support with a fixed angle.

3. Results and discussions

3.1. Comparison of different models in predicting the directional adhesion law

Although the Rivlin model and Kendall model are used to predict the pull-off force of a thin film adhered to a rigid substrate, other than the fiber constrained on a rigid support with a fixed angle, they can also provide acceptable approximations for the latter in some cases. Thus we compare them with the ISCM and ESCM in terms of predicting the directional adhesion law in the same 2D force space. The critical lines of adhesion predicted by different models are displayed in Fig. 3. It is found that when both the axial and the bending deformation are significant (for instance, $EI/\omega l^2=1$, $EA/\omega=100$), only the ESCM gives an accurate prediction. When the applied load is relatively small (compared with the maximum shear force), the adhesion law predicted by the ISCM is in good agreement with that of the ESCM; but their difference will become very significant when the applied load is relatively large. The applicable conditions of different models in predicting the directional adhesion law are systematically concluded in Table 1, which will aid in choosing an appropriate model to interpret the outcomes of directional adhesion tests.

3.2. Comparison between the Kendall model and ESCM in predicting the MNPF

In terms of designing fibrillar adhesives with high adhesion strength, the MNPF as predicted by the Kendall model and ESCM is of our great interest (as shown in Fig. 2, Fig. 3). Hence the influences of the axial and bending stiffness on the MNPF are studied in detail.

It is shown in Fig. 4 that both the MNPFs predicted by the Kendall model and the ESCM increase with EA/ω. The MNPF from the ESCM is smaller than that from the Kendall model for the same EA/ω, but it is also evident that in the case of $EI/\omega l^2 = 0.16$, the two models predict almost the same MNPF. The effect of the bending stiffness on the MNPF is more clearly depicted in Fig. 5. For the same EA/ω, the difference between the MNPFs predicted by the

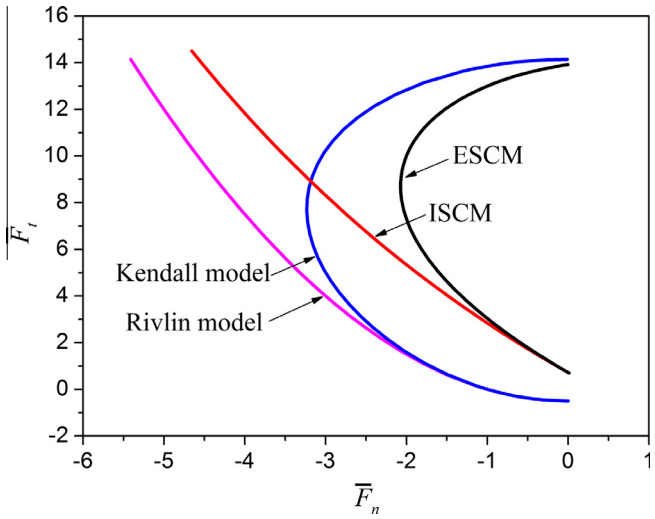

Fig. 3. Comparison of different models in predicting the directional adhesion law where $EI/\omega l^2 = 1$, $EA/\omega = 100$ and $\alpha = 0$.

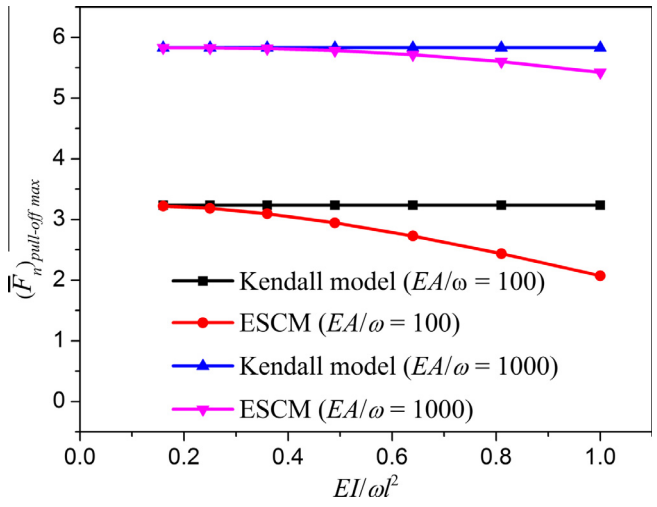

Fig. 5. Effect of the bending stiffness $EI/\omega l^2$ on the maximum normal pull-off force predicted by the extensible side contact model and the Kendall model ($\alpha = 0$).

Table 1
Comparison of different models in predicting the directional adhesion law.

EA/ω	$EI/\omega l^2$	α	Equations
∞	0	$\alpha < \alpha_{cr}$[a]	Rivlin model
∞	0	Any	CLJSC of ISCM
∞	Finite	Any	CLSC of ISCM
Finite	0	$\alpha < \alpha_{cr}$[a]	Kendall model
Finite	0	Any	CLJSC of ESCM
Finite	Finite	Any	CLSC of ESCM

[a] According to Eq. (12) in the reference He et al. (2012) or Eqs. (14) and (15) in this paper, for a given $(F_t)_{min} > 0$, there exists a critical α_{cr} such that F_t at the transitional point on the CLJSC equals $(F_t)_{min}$. Thus if $\alpha < \alpha_{cr}$, the Rivlin model or Kendall model could predict the directional adhesion behavior in the range of $F_t > (F_t)_{min}$.

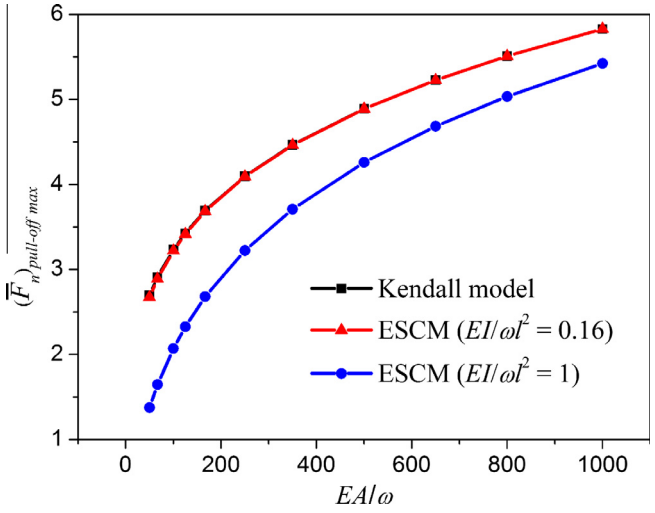

Fig. 4. Effect of the axial stiffness EA/ω on the maximum normal pull-off force predicted by the extensible side contact model and the Kendall model ($\alpha = 0$).

two models respectively increases with the bending stiffness. By comparing the curves shown in Fig. 4, Fig. 5, it is easy to find that within the displayed range of values, the enhancing effect of the axial stiffness on the MNPF is much stronger than the reducing effect of the bending stiffness. Table 2 concludes the applicable conditions of the Kendall model and the ESCM in predicting the MNPF, which is potentially contributive to the structural optimization of fibrillar dry adhesives.

Table 2
Comparison of the Kendall model and the ESCM in predicting the MNPF.

EA/ω	$EI/\omega l^2$	Model
Finite	0	Kendall model
Finite	Small[a]	Kendall model (approximation)
Finite	Finite	ESCM

[a] Here the maximum allowable $EI/\omega l^2$ depends on EA/ω and the required accuracy of the approximation.

It should be pointed out that the range of the values of physical quantities (eg. $EI/\omega l^2$ and EA/ω) could be very wide as long as both the basic assumptions of continuum mechanics and the concept of surface energy are applicable. In order to illustrate the results given by the new ESCM model simply and clearly, we only choose a very limited range of values. Through simple calculations, it is known that the calculated $EI/\omega l^2$ for the gecko's spatula pad (Chen et al., 2008) and a single-level artificial adhesive structure (Lee et al., 2008) are both between 0.2 and 1, and the non-dimensional adhesion and shear forces are within the acceptable range. Therefore, it is expected that the ESCM model could be applied to the adhesion of gecko's spatula pad and the adhesion of single-level artificial adhesive structure.

3.3. Application of the adhesion law to the design of single-level fibrillar adhesives

The conclusion derived above could contribute to the rational design of single-level fibrillar adhesives. Taking the design of a vertical fiber with a rectangular cross-section as an example, we will discuss how to make a rational choice of the aspect ratio (AR) and the cross-sectional area ($A = bh$ where b and h are the width and height of the rectangular cross-section respectively) with the purpose of obtaining a large MNPF. It is assumed that the material properties of the fiber remain constant.

First it can be shown from the following equation

$$\frac{EA/\omega}{EI/(\omega l^2)} = \frac{12bh}{bh^3/l^2} = \frac{12l^2}{h^2} \propto AR^2, \tag{21}$$

that the ratio of the axial stiffness to the bending stiffness only relies on the AR.

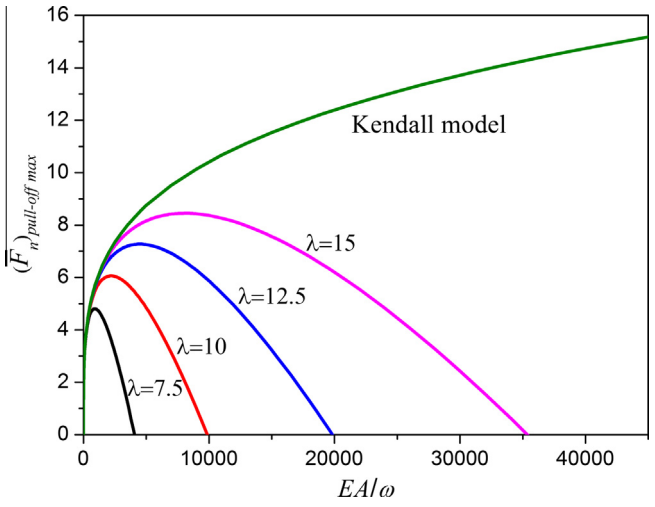

Fig. 6. Effects of the cross-sectional area and aspect ratio ($AR = l/h$) of the fiber on the maximum normal pull-off force with the materials properties remained constant ($\alpha = 0$).

The effect of A on the MNPF for fibers with different ARs is illustrated in Fig. 6. It shows that for a given AR, there exists an optimum axial stiffness so that the MNPF is maximized. This is because, when the axial stiffness is comparatively small, the enhancing effect of the axial stiffness on the adhesion is much stronger than the reducing effect of the bending stiffness, and, as a result, the MNPF increases with the axial stiffness; however, if the axial stiffness exceeds the optimum value, the bending stiffness will become too large and leads to the decrease of the MNPF. Fig. 6 also shows that, in terms of a fiber with a constant A, the MNPF will saturate to the limit set by the Kendall model when AR is large enough. Therefore, only when its AR is large enough or saying the bending stiffness is low enough, could the Kendall model be used to predict the fiber's MNPF.

However, when practical adhesive systems, usually a fiber array, are designed, it is impossible to decrease the bending stiffness of a single fiber too much so as to increase the pull-off force of a single fiber. If the bending stiffness is too small, adjacent fibers would adhere to each other much easier (Spolenak et al., 2005). Therefore when trying to optimize the adhesion force of the fiber array on a unit area, i.e. making the apparent adhesion strength as high as possible, one should first make sure that adjacent fibers do not adhere and the effective stiffness of the fiber array is low enough so that it would easily conform to practical rough surfaces (Greiner et al., 2009; Spolenak et al., 2005). It is probable that an optimal adhesive system is not that with very slender fibers. In this case, one has to utilize the new model in order to accurately predict the achievable adhesion force of the fibers, for a simple adoption of the Kendall model will bring about large errors in predicting the apparent adhesion strength (Greiner et al., 2009).

3.4. Influence of the pre-tension on the directional adhesion behavior

The influence of the pre-tension on the directional adhesion behavior is also studied in detail as shown in Fig. 7. Comparison between different CLJSC in Fig. 7(a) shows that if F_t is small, the normal pull-off force decreases with the increase of the pre-tension; but if F_t is large enough, increasing the pre-tension can effectively enhance the normal pull-force. Moreover, the possible MNPF on the CLJSC increases monotonically with the pre-tension. However, the CLSC as depicted in Fig. 7(b) shows that the actual MNPF does not always increase with the pre-tension and takes a maximum value for some pre-tension. Fig. 7(c) displays this result more clearly,

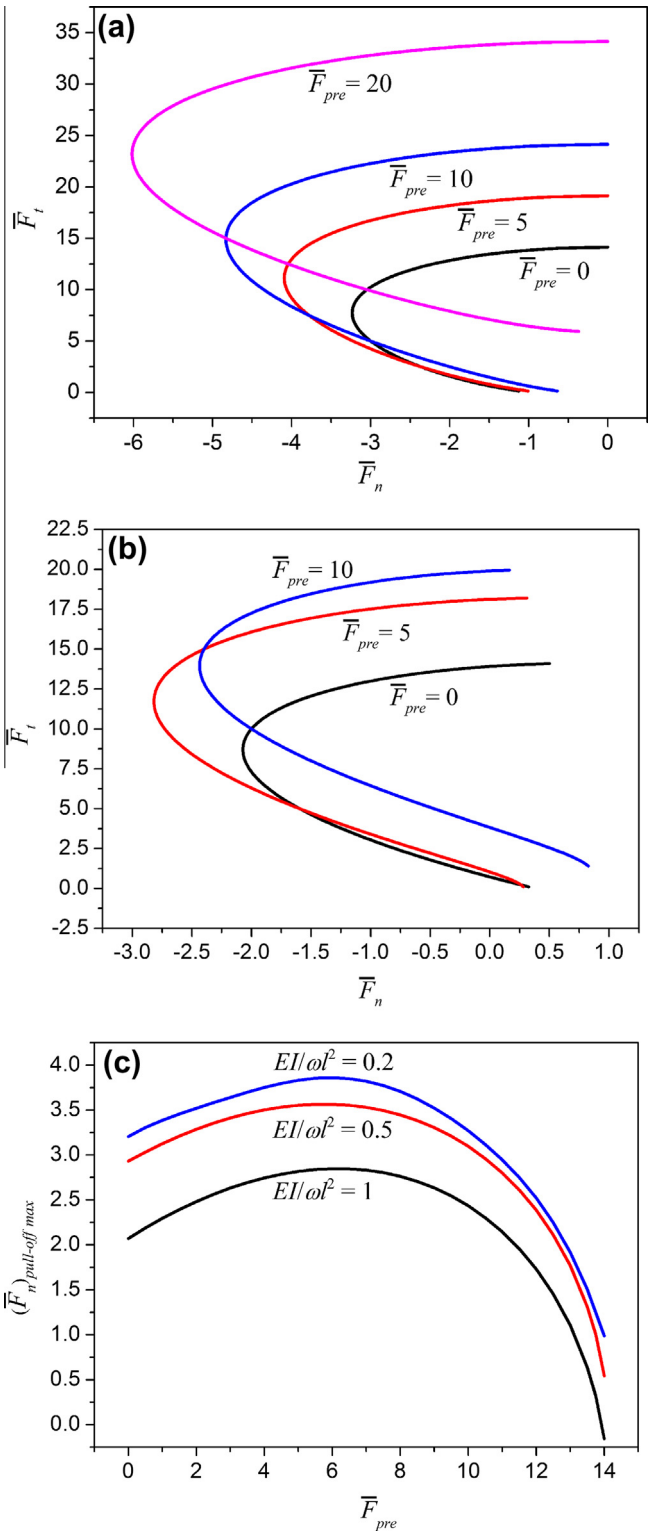

Fig. 7. Influence of the pre-tension in the adhered part of the fiber on the directional adhesion behavior. The critical lines of jumping off side contact for different pre-tensions are shown in (a) ($EI/\omega l^2 = 1$, $EA/\omega = 100$, $\alpha = 0$), and the critical lines of side contact for different pre-tensions are shown in (b) ($EI/\omega l^2 = 1$, $EA/\omega = 100$, $\alpha = 0$). The influence of the pre-tension on the maximum normal pull-off force is sketched in (c) ($EA/\omega = 100$, $\alpha = 0$).

and it also shows that the bending stiffness of the fiber nearly does not affect the "optimal pre-tension". This can be explained as follows: firstly, from Eq. (17) we know that only when the F_{pre} equals F_t or is very close to F_t, would the adhesion property be optimally

enhanced; secondly, the results in Section 2.3 show that the optimal F_t for the pre-tension free fiber to achieve the MNPF strongly depends on the axial stiffness; as a result, the optimal pre-tension needed to maximize the MNPF is very close to the so called optimal F_t and is not decided by the bending stiffness but by the axial stiffness.

Although the pretension effect has not been clearly validated by experimental data, many theoretical and numerical researches do support such a mechanism (Chen et al., 2009; Cheng et al., 2012). Further work needs to be done to validate it experimentally and it may be helpful to inspire the design of biomimetic adhesives and biomimetic climbing robots.

4. Conclusion

An adhesion model for an extensible fiber in side contact with a rigid flat surface is developed to study its directional adhesion behavior. Firstly, the governing equation and the adhesion criterion of the fiber are derived via a variational method. Then its configuration after deformation is obtained analytically. Based on that result, the fiber's directional adhesion law is predicted directly and all its adhesion equilibrium states are found stable. Moreover, the influence of the pre-tension in the adhered part of the fiber on the adhesion behavior can also be naturally incorporated into the model.

It is found that, due to the extensibility of the fiber, there exists a maximum normal pull-off force (MNPF) when an optimal shear force is applied. Detailed studies reveal that the MNPF will be enhanced by increasing the axial stiffness, and reduced by increasing the bending stiffness. Only when the bending stiffness is small enough can the Kendall model be used to predict the MNPF. It is further found that generating an optimal pre-tension can maximize the MNPF, and the optimal value almost is not decided by the bending stiffness, but by the axial stiffness.

By comparing the newly developed extensible side contact model (ESCM) with the Rivlin model, the Kendall model and the inextensible side contact model (ISCM), it is shown that they are degenerate versions of the new model. And their respective applicable conditions in predicting the directional adhesion law are also systematically concluded. Therefore the directional adhesion law of such an extensible fiber and the applicable conditions of these models are expected to contribute to the optimal design and applications of single-level fibrillar adhesives.

Acknowledgments

This work is supported by the National Basic Research Program of China (973 Program, No. 2011CB302101) and the directional project of Hefei physical science and technology center (2012FXCX002)

Appendix The proof for the stability of the adhesion equilibrium states

Firstly according to the definition of strain energy release rate, we obtain

$$G = -\frac{\partial U}{\partial a} = \left[\frac{1}{2}EI\left(\frac{\partial\theta}{\partial s}\right)^2 + \frac{F_{ten}^2}{2EA}\right]\Bigg|_{s=a}. \tag{A.1}$$

By using Eq. (7), Eq. (6) this equation can be reduced to the following form:

$$G = -F_t + M, \tag{A.2}$$

where F_t is a constant and M is a monotonically decreasing function of a.

In order to determine the stability of the adhesion equilibrium states, we need calculate

$$\left[\frac{dG}{da}\right]\Big|_{a=\hat{a}} = \left[\frac{dM}{da}\right]\Big|_{a=\hat{a}}. \tag{A.3}$$

By using Eq. (9), the following derivative can be derived:

$$\frac{da}{dM} = -\sqrt{EI}\int_{\alpha}^{\pi/2}\frac{d\theta}{[2M - 2N\sin(\theta-\phi) + N^2c\sin^2(\theta-\phi)]^{3/2}}. \tag{A.4}$$

Thus

$$\left[\frac{dM}{da}\right]\Big|_{a=\hat{a}} = -\frac{1}{\sqrt{EI}}\frac{1}{\Gamma}, \tag{A.5}$$

where

$$\Gamma = \int_{\alpha}^{\pi/2}\frac{d\theta}{[2\hat{M} - 2N\sin(\theta-\phi) + N^2\sin^2(\theta-\phi)/(EA)]^{3/2}} > 0.$$

Finally substituting (A.5) into Eq. (A.3), we have:

$$\left[\frac{dG}{da}\right]\Big|_{a=\hat{a}} = -\frac{1}{2\sqrt{EI}}\frac{1}{\Gamma} < 0. \tag{A.6}$$

Therefore all the available adhesion equilibrium states are stable. The CLJSC is also the critical line of stable adhesion. This conclusion is the same with that of the inextensible case (He et al., 2012).

References

Arzt, E., Gorb, S., Spolenak, R., 2003. From micro to nano contacts in biological attachment devices. Proc. Nat. Acad. Sci. USA 100, 10603–10606.
Autumn, K., Sitti, M., Liang, Y.A., Peattie, A.M., Hansen, W.R., Sponberg, S., et al., 2002. Evidence for van der Waals adhesion in gecko setae. Proc. Nat. Acad. Sci. USA 99, 12252.
Autumn, K., Dittmore, A., Santos, D., Spenko, M., Cutkosky, M., 2006. Frictional adhesion: a new angle on gecko attachment. J. Exp. Biol. 209, 3569–3579.
Carbone, G., Pierro, E., Gorb, S.N., 2011. Origin of the superior adhesive performance of mushroom-shaped microstructured surfaces. Soft Matter 7, 5545–5552.
Chen, B., Wu, P.D., Gao, H., 2008. Hierarchical modelling of attachment and detachment mechanisms of gecko toe adhesion. Proc. R. Soc. A 464, 1639–1652.
Chen, B., Wu, P., Gao, H., 2009. Pre-tension generates strongly reversible adhesion of a spatula pad on substrate. J. R. Soc. Interface 6, 529–537.
Cheng, Q., Chen, B., Gao, H., Zhang, Y., 2012. Sliding-induced non-uniform pre-tension governs robust and reversible adhesion: a revisit of adhesion mechanisms of geckos. J. R. Soc. Interface 9, 283–291.
del Campo, A., Greiner, C., Arzt, E., 2007. Contact shape controls adhesion of bioinspired fibrillar surfaces. Langmuir 23, 10235–10243.
Federle, W., Riehle, M., Curtis, A.S.G., 2002. An integrative study of insect adhesion: mechanics and wet adhesion of pretarsal pads in ants. Integr. Comp. Biol. 42, 1100–1106.
Gao, H.J., Yao, H.M., 2004. Shape insensitive optimal adhesion of nanoscale fibrillar structures. Proc. Nat. Acad. Sci. USA 101, 7851–7856.
Greiner, C., Spolenak, R., Arzt, E., 2009. Adhesion design maps for fibrillar adhesives: the effect of shape. Acta Biomater 5, 597–606.
He, L.W., Yan, S.P., Li, B.Q., Chu, J.R., 2012. Directional adhesion behavior of a single elastic fiber. J. Appl. Phys. 112, 013516.
Hui, C.Y., Glassmaker, N.J., Tang, T., Jagota, A., 2004. Design of biomimetic fibrillar interfaces: 2. Mechanics of enhanced adhesion. J. R. Soc. Interface 1, 35–48.
Jagota, A., Bennison, S.J., 2002. Mechanics of adhesion through a fibrillar microstructure. Integr. Comp. Biol. 42, 1140–1145.
Jeong, H.E., Lee, J.-K., Kim, H.N., Moon, S.H., Suh, K.Y., 2009. A nontransferring dry adhesive with hierarchical polymer nanohairs. Proc. Nat. Acad. Sci. USA 106, 5639–5644.
Jeong, H.E., Lee, J.-K., Kwak, M.K., Moon, S.H., Suh, K.Y., 2010. Effect of leaning angle of gecko-inspired slanted polymer nanohairs on dry adhesion. Appl. Phys. Lett. 96, 043704.
Johnson, K., 1985. Contact Mechanics. Cambridge University Press, Cambridge.
Kendall, K., 1975. Thin-film peeling – elastic term. J. Phys. D: Appl. Phys. 8, 1449–1452.
Kim, T.I., Jeong, H.E., Suh, K.Y., Lee, H.H., 2009. Stooped nanohairs: geometry-controllable, unidirectional, reversible, and robust gecko-like dry adhesive. Adv. Mater. 21, 2276–2281.
Lee, J., Majidi, C., Schubert, B., Fearing, R.S., 2008. Sliding-induced adhesion of stiff polymer microfibre arrays. I. Macroscale behaviour. J. R. Soc. Interface 5, 835–844.
Liu, J., 2009. Adhesion and Friction of a Bio-inspired Dry Adhesive and Van der Waals Interactions, Cornell University: Doctor of Philosophy.

Magnusson, A., Ristinmaa, M., Ljung, C., 2001. Behaviour of the extensible elastica solution. Int. J. Solids Struct. 38, 8441–8457.
Majidi, C.S., 2009. Shear adhesion between an elastica and a rigid flat surface. Mech. Res. Commun. 36, 369–372.
Majidi, C.S., Groff, R.E., Fearing, R.S., 2005. Attachment of fiber array adhesive through side contact. J. Appl. Phys. 98, 103521.
Murphy, M.P., Aksak, B., Sitti, M., 2009. Gecko-inspired directional and controllable adhesion. Small 5, 170–175.
Peng, Z.L., Chen, S.H., Soh, A.K., 2010. Peeling behavior of a bio-inspired nano-film on a substrate. Int. J. Solids Struct. 47, 1952–1964.
Pesika, N.S., Tian, Y., Zhao, B., Rosenberg, K., Zeng, H., McGuiggan, P., et al., 2007. Peel-zone model of tape peeling based on the gecko adhesive system. J. Adhes. 83, 383–401.
Qu, L., Dai, L., Stone, M., Xia, Z., Wang, Z.L., 2008. Carbon nanotube arrays with strong shear binding-on and easy normal lifting-off. Science 322, 238–242.
Rivlin, R.S., 1944. The effective work of adhesion. Paint Technol. 9, 215–216.
Soto, D., Hill, G., Parness, A., Esparza, N., Cutkosky, M., Kenny, T., 2010. Effect of fibril shape on adhesive properties. Appl. Phys. Lett. 97, 053701.
Spolenak, R., Gorb, S., Arzt, E., 2005. Adhesion design maps for bio-inspired attachment systems. Acta Biomater. 1, 5–13.
Tian, Y., Pesika, N., Zeng, H., Rosenberg, K., Zhao, B., McGuiggan, P., et al., 2006. Adhesion and friction in gecko toe attachment and detachment. Proc. Nat. Acad. Sci. USA 103, 19320–19325.
Timoshenko, S.P., Gere, J.M., 1962. Theory of Elastic Stability. McGraw-Hill, New York.
Varenberg, M., Pugno, N.M., Gorb, S.N., 2010. Spatulate structures in biological fibrillar adhesion. Soft Matter 6, 3269–3272.
Yoon, H., Jeong, H.E., Kim, T.-i., Kang, T.J., Tahk, D., Char, K., Suh, K.Y., 2009. Adhesion hysteresis of Janus nanopillars fabricated by nanomolding and oblique metal deposition. Nano Today 4, 385–392.